XBn and XBp infrared detectors

P.C. Klipstein,

SemiConductor Devices P.O. Box 2250, Haifa 31021, Israel

XBn and XBp barrier detectors grown from III-V materials on GaSb substrates have recently been shown to exhibit a low diffusion limited dark current and a high quantum efficiency (QE). Two important examples are InAsSb/AlSbAs based XBn devices with a cut-off wavelength of λ_C ~ 4.1 μm, and InAs/GaSb type II superlattice (T2SL) based XBp devices, with λ_C ~ 9.5 μm. The former exhibit background limited performance (BLIP) at F/3 up to nearly 200 K, which is a much higher temperature than observed in standard generation-recombination (G-R) limited devices such as InSb photodiodes, operating in the same Mid Wave IR (MWIR) atmospheric window. The Long Wave IR (LWIR) T2SL XBp device has a BLIP temperature of ~100K at F/2. Using the **k · p** and optical transfer matrix methods, full spectral response (SR) curves of both detectors can be predicted quite accurately from a basic knowledge of the layer thicknesses and doping. The SR curves of LWIR gallium free InAs / $InAs_{1-x}Sb_x$ XBn and XBp devices have also been simulated. These devices have a lower QE than the equivalent InAs/GaSb XBp device, due to their lower absorption coefficients. In the XBn case, a small diffusion length is also expected, which may further reduce the QE.

Keywords: Infrared Detector, Focal Plane Array, Type II superlattice, Gallium free superlattice, Bariode, XBn, XBp, pBp, LWIR.

1. INTRODUCTION

High performance photodiode Focal Plane Array (FPA) detectors that operate in the Mid or Long Wave Infra-Red (MWIR or LWIR) "window" of the atmosphere are often made from Mercury Cadmium Telluride (MCT), because of the potential tunability of the band gap and the low "diffusion" limited dark current[1]. However, the need for high quality Cadmium Zinc Telluride (CZT) substrates makes them expensive and difficult to scale to large areas. For this reason InSb FPAs are often preferred in the MWIR, even though they must operate a few tens of degrees colder, in order to suppress the generation-recombination (G-R) current created in the photodiode depletion region[2]. Recently, InAs/GaSb Type II superlattices (T2SLs) have emerged as another competitor to MCT because, like MCT, they also offer tunability over the full MWIR and LWIR ranges.

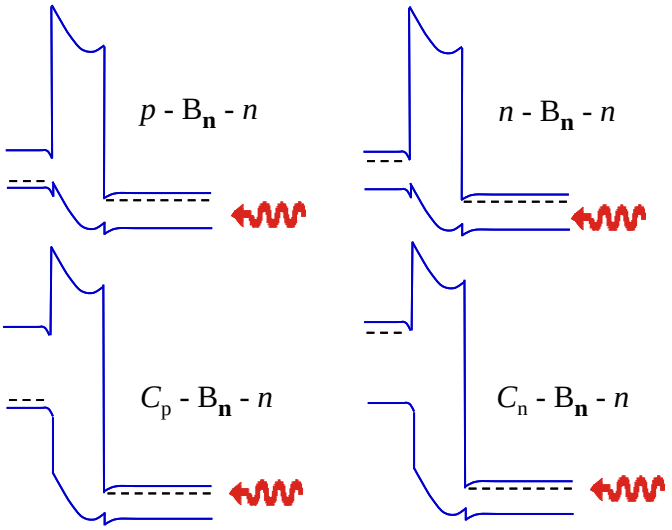

Figure 1
The four contact configurations of an *n*-type bariode device with an *n*-type InAsSb active layer ("*n*") on the right hand side of an *n*-type AlSbAs barrier layer ("B_n"). In the upper row the contact layer (X) on the left of the barrier is InAsSb while in the lower row it is GaSb. In the left hand column the contact is *p*-type (X= "*p*" or "C_p") while in the right hand column it is *n*-type (X= "*n*" or "C_n"), making the devices in this column unipolar.

Although they are also G-R limited, the G-R problem has recently been overcome using a patented XB*n*/XB*p* technology[3,4] which can be implemented in the MWIR or LWIR in III-V devices grown on commercial GaSb substrates. It provides a low diffusion limited dark current as in MCT, but with many of the advantages of III-V materials, including the potential for scalability to large areas at affordable cost.

2. XBn DEVICES

Schematic band diagrams for an InAsSb XB$_n$n detector[5], are shown in Figure 1. The detector has a cut-off wavelength close to 4.1 μm and is based on a heterostructure design that can be grown with high quality on GaSb or even GaAs[6] substrates, using Molecular Beam Epitaxy (MBE). The device contains an *n*- or *p*-type contact layer made from InAs$_{1-x}$Sb$_x$ or GaSb (X), a barrier layer made from *n*-type AlSb$_{1-y}$As$_y$ (B$_n$), and an active layer made from *n*-type InAs$_{1-x}$Sb$_x$ (n). By excluding the depletion region from the photon absorbing layer the G-R current is strongly suppressed. This is achieved by ensuring that the barrier and photon absorbing layers are both doped *n*-type, and creates the interesting situation of a completely unipolar *n*B$_n$*n* device which behaves in many ways like a photovoltaic detector with a gain of one, even though it contains no *p*-*n* junction[4].

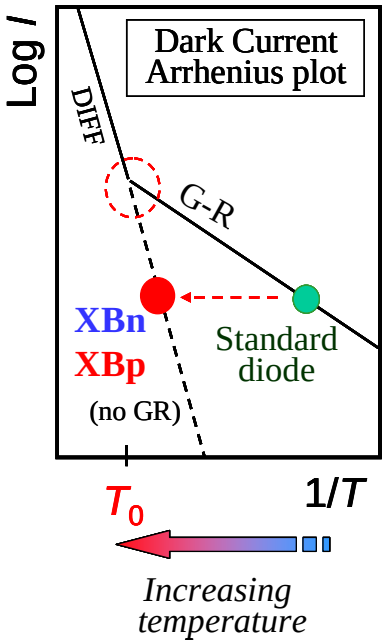

Figure 2
Schematic T-dependence of I_{dark} in a *p*-*n* diode (green dot) and a XB$_n$*n* or XB$_p$*p* barrier detector (red dot) with the same active layer

When the G-R current is suppressed, the result is a large increase in operating temperature for a detector with a given dark current, as depicted by the red arrow in Figure 2. As shown in the Figure, the G-R current is activated with approximately half the energy of the diffusion current. The two contributions are equal at the crossover temperature T_0, which increases with the active layer (AL) band gap energy[7]. The effect of changing the barrier layer (BL) polarity is shown in Figure 3. If the barrier has the opposite doping polarity to the photon absorbing layer, then a depletion region develops in the photon absorbing layer and a large G-R current ensues. Figure 3 shows two nominally identical devices with opposite barrier polarities, each operating at a bias of -0.1 V. The *n*B$_n$*n* device exhibits a single straight line, characteristic of diffusion limited behaviour, while the *n*B$_p$*n* device exhibits two slope behaviour, characteristic of a crossover from diffusion limited behaviour at high temperatures to G-R limited behaviour at low temperatures. The dark current at 150 K (enlarged points in Figure 3) is 100× greater for the detector with the *p*-type barrier because it is already G-R limited. For a typical quantum efficiency of 70% at F/3, this results in a lower background limited performance (BLIP) temperature of ~140 K, compared with ~175 K for the detector with the *n*-type barrier.

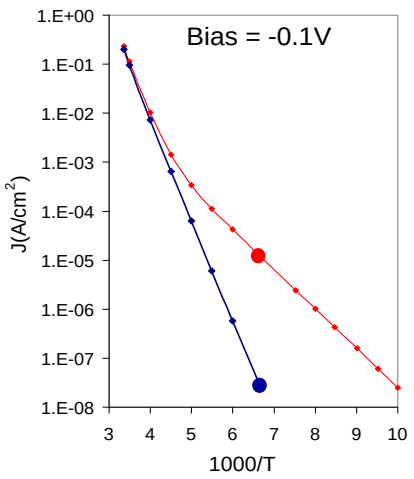

Figure 3
Log J_{dark} vs 1000/T for identical InAsSb/AlSbAs *n*B*n* devices but with opposite barrier doping polarities (red = *p*, blue = *n*). Active layer bandgap wavelength, λ_G = 4.1 μm at 150K

Figure 4 shows a series of images registered at F/3.2 and different operating temperatures up to 225 K for a 15 μm pitch FPA detector flip-chip bonded to SCD's Pelican-D 640 × 512 Silicon Read-Out Integrated circuit (ROIC). The FPA has a quantum efficiency (QE) of ~ 80%. There is no discernable degradation in image quality until ~193 K, as expected for a BLIP temperature of ~175 K. Such high imaging temperatures, up to nearly 200 K, allow considerable

reductions in size, weight and power of the complete integrated XB_nn detector/cooler assembly. Further details of the radiometric performance of these XBn detectors may be found in Refs. 8, 9

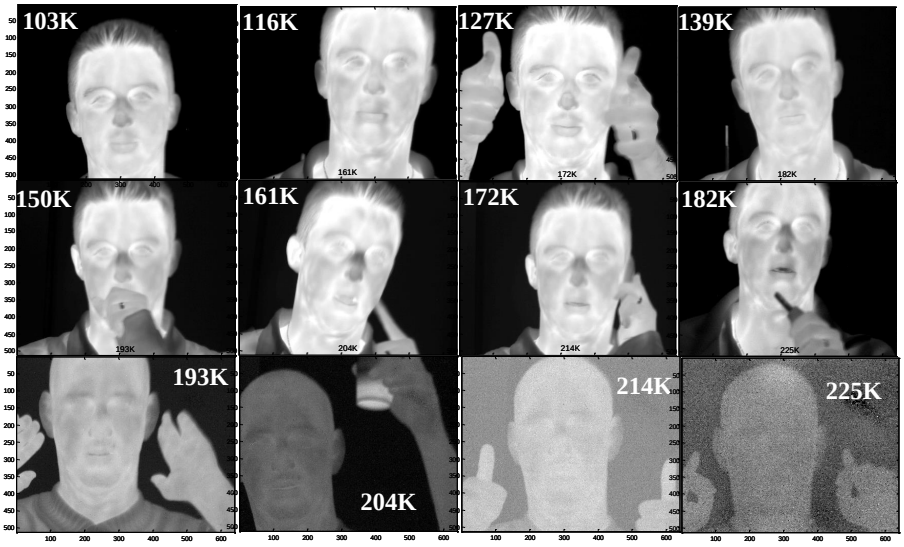

Figure 4
Images at FPA temperatures between 103 and 225 K, for a 640 × 512 XBn FPA at F/3.2.

3. XBp DEVICES

Figure 5 (a) shows a schematic band structure for the BL and AL of an XB*p* device based on InAs/GaSb and InAs/AlSb T2SLs. In (b) the edges of the mini-bands shown in (a) are sketched for an operating pB_pp device, where all layers are doped *p*-type. The advantage of the barrier device is demonstrated in Figure 6, which compares a standard LWIR *n*-on-*p* diode based solely on InAs/GaSb, with a LWIR pB_pp device based on the design in Figure 5.

Both devices have an AL band gap wavelength close to 10 μm. The barrier device (blue) is diffusion limited down to 77K, while the diode is G-R limited at this temperature, with a dark current over 20× larger. The dark current in our pB_pp devices is within one order of magnitude of MCT Rule-07[10], which is the performance standard for state of the art Mercury Cadmium Telluride (MCT) photo-diodes.

The full spectral response for an FPA made from the pB_pp device shown in Figure 5 (b) can be simulated if the thickness of the InAs and GaSb layers in the T2SL period are known. The simulation is based on a **k** · **p** treatment and optical transfer matrix calculation recently reported elsewhere[11]. Figure 7 compares the simulated and measured QE values at 77K (weighted by the 300 K black body spectrum and

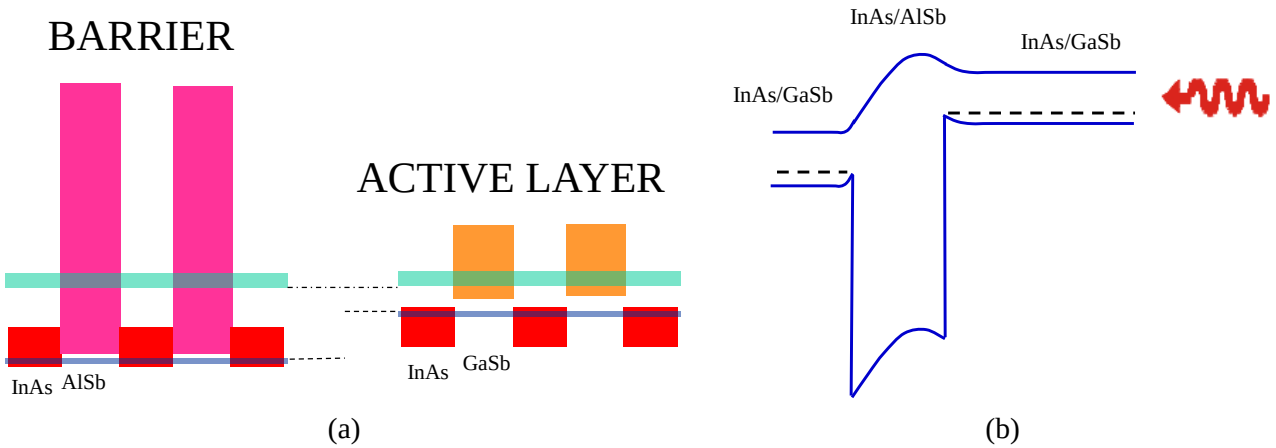

Figure 5
(a) Alignment between mini-bands in the active and barrier layers of a T2SL XB*p* device, super-imposed on the bandgaps of InAs, GaSb and AlSb (b) Schematic profile of band edges in an operating *p*B*p* device, based on the minibands shown in a)

averaged over a spectral window of 7.6 – 9.5 μm) for a series of LWIR pB_pp test devices with AL thickness values from 1.5 – 6.0 μm and a cut-off wavelength of ~ 9.5 μm. The solid line is for the simulation when no anti-reflection coating (ARC) is used and the dashed line is when an ARC is used. The detector structures include a mirror on the contact layer (CL) to reflect 80% of the light back for a second pass. Measured QE values are shown as points and they all appear quite close to the respective simulated curves. Details of the method of measurement are given in Ref. 12.

The inset in Figure 7 shows the typical bias dependence of the QE at 77 K for a 100×100μm^2 test device. The signal does not reach its full value until ~0.6V, when the bias has reduced the hump-like barrier in the conduction band enough to allow photo-generated minority electrons to pass freely from the AL to the CL (See Figure 5 (b)). This behavior is typical of XBn and XBp barrier devices and highlights the dependence of the operating bias (V_{OP}) on barrier doping (N_A) and width (W). Both of these parameters increase the height of the hump-like barrier for minority carriers and thus increase the operating bias. The operating bias varies approximately as $V_{OP} = V_0 + N_A W^2$, where V_0 is a constant.

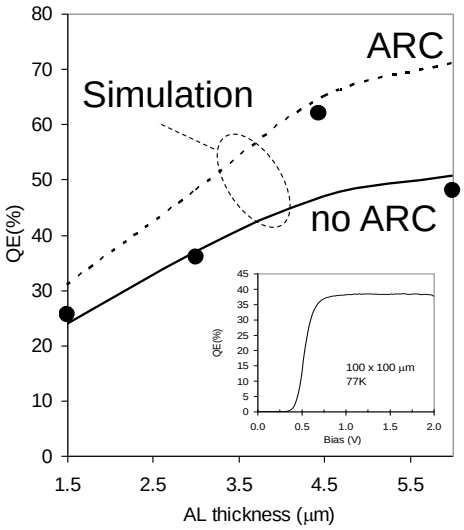

Figure 7
Simulated (lines) and measured (dots) QE values at 77K for LWIR pB_pp test devices with AL thicknesses from 1.5 – 6.0 μm and a cut-off wavelength of ~9.5 μm. An anti-reflection coating (ARC) is included for the dashed line. A mirror on the contact layer reflects 80% of the light back for a second pass. *Inset:* Example of QE vs bias.

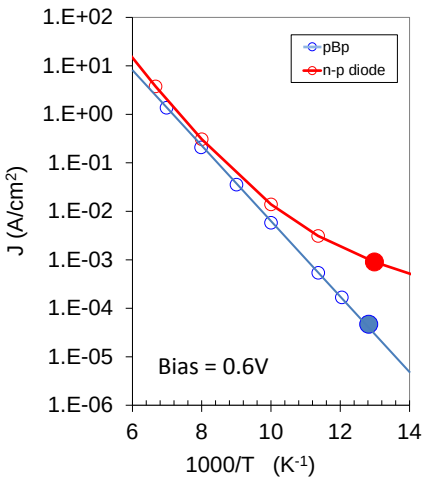

Figure 6
Log J_{dark} vs. 1000/T in pB_pp barrier device and *n-p* diode, each with an InAs/GaSb active layer bandgap wavelength of λ_G ~ 10 μm (mesa area = 100×100 μm^2)

It has recently been proposed that gallium free, InAs/InAs$_{1-x}$Sb$_x$ T2SLs may offer better detector performance because they exhibit minority carrier lifetimes about one order of magnitude greater than InAs/GaSb T2SLs[13]. Figure 8 compares 77 K measured and simulated absorption spectra for two MWIR T2SL structures with similar cut-off wavelengths: (a) an 8.4/13.7 InAs/GaSb T2SL and (b) 12.8/12.8 InAs/InAs$_{0.815}$Sb$_{0.185}$ T2SL (thicknesses in monolayers). In the second case, the conduction and valence band bowing parameters had to be found that gave the best agreement with both bulk and T2SL band gaps[11]. The results demonstrate that the simulations are quite faithful to the measurements, and that the gallium free T2SL exhibits a weaker absorption coefficient near the cut-off wavelength.

The spectral response of a 35/12 InAs/InAs$_{1-x}$Sb$_x$ (x=0.41) T2SL CBp detector with a band gap wavelength of ~16 μm at 77K was recently reported by Hoang et al.[14] The BL was a 35/6 InAs/AlSb T2SL similar to those simulated by the **k · p** model in Ref. 11. Figure 9 shows our simulation of the spectral response of this CBp structure. It was assumed that the device had an antireflection coating. In the simulation it was necessary to increase the antimony concentration in the ternary layer by 2% (x=0.43) in order to obtain a good match to the band gap. The shape of the curve and maximum QE match those in Ref. 14 quite well.

In Figure 10, the spectral response has been calculated at 77 K for two pBp detectors, based on a 13.8/7 InAs/GaSb T2SL and a 31.5/9.5 $InAs/InAs_{1-x}Sb_x$ (x=0.39) T2SL, respectively. They both have a cut-off wavelength of 9.9 μm. In each case

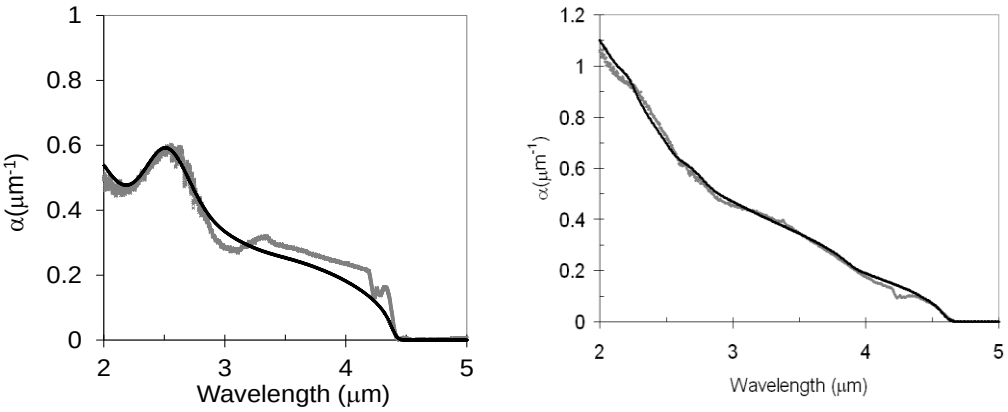

Figure 8
Meaured (grey) and simulated (black) absorption at 77K for : (a) an 8.4/13.7 InAs/GaSb T2SL and (b) 12.8/12.8 $InAs/InAs_{0.815}Sb_{0.185}$ T2SL

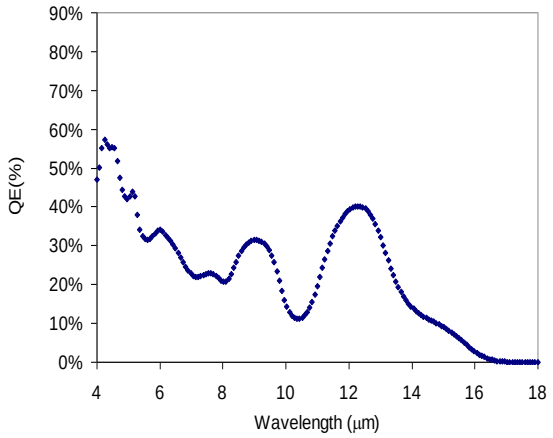

Figure 9
Simulated spectral response at 77K for a CBp device similar to that reported in Ref. 14

the BL used is an InAs/AlSb T2SL, with layer thicknesses of 17/4 and 50/8 respectively. In the former case there is a smooth conduction band and a valence band barrier (VBB) of ~1.9× the AL band gap, which is an ideal arrangement for an XBp device where the VBB should be at least equal to the AL band gap. For the gallium free device the VBB is only 0.7× the AL band gap, and there is a small conduction band barrier (CBB). For such a device the G-R current will exhibit an activation energy of roughly 0.85× the AL bandgap, and it will be characteristic of an InAs/AlSb T2SL, which may have quite a short G-R lifetime. This pB_pp device is therefore not ideal, due to the lack of a taller BL. Nevertheless, the spectral response has been calculated for both devices, assuming that all of the photo-generated electrons can diffuse to the CL and be collected (diffusion length, $L_D >>$ AL thickness, t_{AL}). This is a reasonable assumption since the effective mass of the electrons is quite low in both structures. It was assumed that 80% of the light is reflected back for a second pass by a mirror on the top of the device, that there is an antireflection coating, and that t_{AL} =5μm. It can be seen that the QE of the gallium free device is significantly lower than that of the InAs/GaSb T2SL, with average values over the 7.6 - 9.9μm range of 40% and 70%, respectively. The lower value in the $InAs/InAs_{1-x}Sb_x$ T2SL is related to its weaker absorption coefficient.

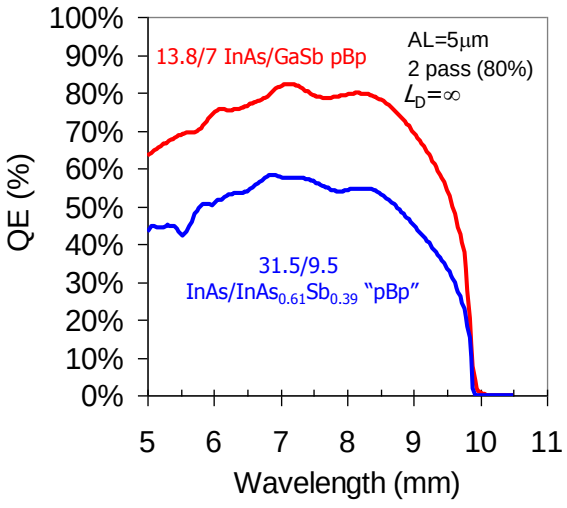

Figure 10
Simulated spectral response for pBp detectors based on a 13.8/7 InAs/GaSb T2SL (red) and a 31.5/9.5 $InAs/InAs_{1-x}Sb_x$ (x=0.39, blue). 80% of the light is reflected back for a second pass and t_{AL} = 5μm.

In order to make an InAs/$InAs_{1-x}Sb_x$ T2SL barrier device with a taller barrier, an *n*B_n*n* structure can be used, with an AlGaSbAs alloy BL. The CBB is then many times greater than the AL bandgap. However, the detector then suffers from a low minority carrier mobility due to the very large effective mass of the holes. This case has been discussed in detail in Ref. 11. While there will be a low diffusion limited dark current from the InAs/$InAs_{1-x}Sb_x$ AL, the QE is likely to be reduced significantly from that shown in Figure 10, due to poor carrier collection.

4. SUMMARY

MWIR XBn and LWIR XBp barrier devices have been fabricated from InAsSb/AlSbAs and InAs/GaSb T2SL heterostructures, respectively. In each case it has been possible to achieve a high QE and a diffusion limited dark current close to the MCT Rule-07 value. This has led to a high BLIP temperature of nearly 200K at F/3 for the MWIR device, and ~100K at F/2 for the LWIR device. The performance of an InAs / $InAs_{1-x}Sb_x$ T2SL barrier device with a band gap wavelength of 16 μm has also ben simulated, and found to agree with recently reported data on similar devices. For such long wavelengths it is possible to design an XBp device with a InAs/AlSb T2SL BL that has a VBB greater than the AL bandgap. This is a necessary condition for a low diffusion limited dark current. When the cut-off wavelength is reduced to ~10 μm, the VBB already appears to be smaller than the AL band gap, which may result in a relatively large dark current. The dark current may be reduced by going to an XBn architecture where a AlGaSbAs alloy can be used to make a very tall BL. However, in both cases the QE is expected to be lower than for an InAs/GaSb T2SL detector, due to the smaller absorption coefficient of the InAs/$InAs_{1-x}Sb_x$ T2SL. In the second case, the small hole mobility will result in a small minority carrier diffusion length. This is likely to reduce the QE even more.

ACKNOWLEDGEMENTS

I am grateful to many colleagues, too numerous to mention, whose creativity and dedicated effort in crystal growth, device fabrication and radiometric characterization lead to the results presented here. I am grateful to Dr. M Katz, Dr. Noam Sicron and Mr. Ohad Weistrich of the Soreq Research Centre for processing the n^+-p diode wafer into test devices, and for measuring their dark current as a function of temperature.

REFERENCES

[1] W.E. Tennant, 2009 U.S. Workshop on the Physics & Chemistry of II-VI materials, Chicago, 2009

[2] A. Glozman, E. Harush, E. Jacobsohn, O. Klin, P.C. Klipstein, T. Markovitz, V. Nahum, E. Saguy, J. Oiknine-Schlesinger, I. Shtrichman, M. Yassen, B. Yofis, and E. Weiss, Proc. SPIE **6206**, 6206-0M, 2006

[3] P.C. Klipstein, *Depletionless Photodiode with Suppressed Dark Current*…, US Patent 7,795,640 (2 July 2003)

[4] P.C. Klipstein, *Unipolar semiconductor photodetector with Suppressed Dark Current*…, US Patent 8,004,012 (6 April 2006)

[5] P.C. Klipstein, *X*B*n Barrier Photodetectors for High Sensitivity and High Operating Temperature Infrared Sensors*, Proc. SPIE **6940**, 6940-2U, 2008

[6] E. Weiss, O. Klin, S. Grossmann, N. Snapi, I. Lukomsky, D. Aronov, M. Yassen, E. Berkowicz, A. Glozman, P.C. Klipstein, A. Fraenkel, and I. Shtrichman, Journal of Crystal Growth, **339**, 2012, Pages 31-35

[7] P.C. Klipstein, Proc. SPIE **6940**, 6940-2U (2008)

[8] P.C. Klipstein, Y. Gross, D. Aronov, M. ben Ezra, E Berkowicz, Y. Cohen, R. Fraenkel, A. Glozman, S. Grossman, O. Klin, I. Lukomsky, T. Markowitz, L. Shkedy, I. Strichman, N. Snapi, A. Tuito,, M. Yassen, E. Weiss, Proc. SPIE **8704**, 8704-1S (2013)

[9] Y. Karni, E. Avnon, M. ben Ezra, E. Berkowicz, O. Cohen, Y. Cohen, R. Dobromislin, I. Hirsh, O. Klin, P.C. Klipstein, I. Lukomsky, M. Nitzani, I. Pivnik, O. Rozenberg, I. Shtrichman, M. Singer, S. Sulimani, A. Tuito, E. Weiss, Proc. SPIE **9070**, 9070-1F (2014)

[10] P.C. Klipstein, E. Avnon, Y. Benny, R Fraenkel, , A. Glozman, S. Grossman, O. Klin, L. Langoff, Y. Livneh, I Lukomsky, M. Nitzani, L. Shkedy, I. Shtrichman, N. Snapi, A. Tuito and E. Weiss, Proc. SPIE **9070**, 9070-0U (2014)

[11] P.C. Klipstein, Y. Livneh, A. Glozman, S. Grossman, O. Klin, N. Snapi and E. Weiss, Journal of Electronic Materials, **43**, 2984 (2014)

[12] P.C. Klipstein, O. Klin, S. Grossman, N. Snapi, I. Lukomsky, D. Aronov, M. Yassen, A. Glozman, T. Fishman, E. Berkowicz, O. Magen, I. Strichman, E. Weiss, Optical Engineering **50**, 061002 (2011)

[13] E. H. Steenbergen, B. C. Connelly, G. D. Metcalfe, H. Shen, M. Wraback, D. Lubyshev, Y. Qiu, J. M. Fastenau, A. W. K. Liu, S. Elhamri, O. O. Cellek and Y.-H. Zhang., Appl. Phys. Lett. **99**, 251110 (2011)

[14] A.M. Hoang, G. Chen, R. Chevallier, A. Haddadi and M. Razeghi, Appl. Phys. Lett. **104**, 251105 (2014)